

THE EFFECT OF SATELLITE FORMATION FLYING ON AUTONOMOUS NAVIGATION

Yi Wang, Xiaoqian Chen, Yong Zhao, Yuzhu Bai*

College of Aerospace Science and Engineering, National University of Defense Technology, Changsha 410073, China

Keywords: *autonomous navigation, satellite formation flying, UKF, Monte-Carlo simulation*

Abstract

Combining the technologies of the satellite formation flying with the satellite to satellite tracking (SST), the effect of satellite formation flying on autonomous navigation is analyzed in this paper. Considering the effect of satellite formation flying, the autonomous navigation system with relative inertial-position vector measurement is proposed firstly. Then, observability of the system with the available measurements is investigated using the linear observability analysis, and the absolute state variable observability is obtained, excepting for quite a few special situations. Using Unscented Kalman filter(UKF), the accuracies of state estimation in different satellite formation flying, such as collinear formation, projection circular formation, space circular formation and Along-Cross-Radial(ACR)-Cartwheel formation, is investigated. It can be concluded from the analysis that the collinear formation flying is unobservable, and the ACR-Cartwheel formation flying is more effective and efficient in dealing with autonomous navigation problem. Lastly, the results are confirmed through the Monte-Carlo simulation.

1 Introduction

Autonomous navigation has received much attention in recent years due to the prosperous lunar exploration and deep-space exploration [1-2]. Only using onboard measurement information, the autonomous navigation system is allowed to operate on its own for some length of time to achieve the desired flyby, impact, or soft-landing conditions [3]. While the spacecraft

flying in back lunar or deep space environment, the ground stations are losing communication with spacecraft, and hence the autonomous navigation system is in urgent need to guarantee the mission normal operation. Additionally, the autonomous navigation system could improve the survivability in hostile environment and reduce the costs of the ground-station system and Deep Space Network (DSP) [4].

But compared with the traditional navigation method, the accuracy of autonomous navigation system is lower, so how to improve the orbiting accuracy of the autonomous navigation has become a critical and essential technology in designing the systems. Several enhancements to the current autonomous navigation system would greatly increase its precision and capability to a broader set of missions: Markley [5] and Psiaki [6] designed a batch filter to autonomously determine the orbits of two spacecraft based on measurements of the relative inertial-position vector from one spacecraft to the other. Using the pseudo-range observations from inter-satellite links together with the time difference of arrival measurements, Xiong et al [7] propose a method to determine the absolute position of satellites in constellation. In terms of X-ray pulsar-based navigation and Sun et al [8] combined the star sensor and an ultraviolet earth sensor to realize the autonomous navigation, Wang et al [9] reduce the influence of the planetary ephemerides errors on X-ray pulsar-based navigation system to improve navigational accuracy; Aiming at the low accuracy using extended Kalman filter in case of autonomous navigation, a switch-mode information fusion filter is proposed by Yang et al [10] to ensure the accuracy of the estimation. Based on adaptive sample-

size Gaussian swarm optimization, Maryam et al [11] propose a novel heuristic filter to achieve accurate orbit determination. Shen et al [12] design two types of quantum sensors to increase the accuracy of orbit determination for satellite formation flying.

Surveying from literatures, several enhancements to the current autonomous navigation system would be handled to increase its accuracy: 1) augmentation of data types [5-8]; 2) intensification capability to the filtering algorithms [10-11]; 3) enhancement in error checking and handing [9]; 4) improvement in other interfaces to autonomous navigation [12]. Compared with prior mentioned enhancements, a novel intensification method selecting the available spacecraft formation flying to increase the navigational precision is proposed. Considering the effect of satellite formation flying, the autonomous navigation system with relative inertial-position vector measurement is proposed firstly. Then, observability of the system with the available measurements is investigated using the linear observability analysis, and the absolute state variable observability is obtained, excepting for quite a few special situations. Using Unscented Kalman filter(UKF), the accuracies of state estimation in different satellite formation flying, such as collinear formation, projection circular formation, space circular formation and Along-Cross-Radial(ACR)-Cartwheel formation, is investigated. This process of autonomous system could not add the data types and reduce the onboard payload to save fuel and cost. More importantly, using the optimal formation flying, it could achieve higher accuracy of autonomous navigation.

This paper is organized in five sections. After the introduction, the dynamics model of spacecraft formation flying and measurement model are defined in Section 2. Then, unscented Kalman filter and the observability analysis method are introduced in Section 3. In Section 4, the observability of autonomous system in different satellite formation flying is investigated and the results are confirmed through the Monte-Carlo simulation. Lastly, the conclusion is presented in Section 5.

2 Mathematic modeling

The moon-centered inertial Cartesian coordinate system (J2000.0) [13] and the local vertical local horizontal frame (LVLH) are selected in this paper. And the LVLH frame is centered at the target spacecraft's center of mass, the x-axis points out radially from the center of the Lunar to the center of mass of the leader satellite, the y-axis is aligned in the direction of in-track motion, and the z-axis is normal to the orbital plane. The dynamic model of the autonomous navigation system is given as follows:

$$\begin{bmatrix} \dot{\mathbf{r}}_i \\ \dot{\mathbf{v}}_i \end{bmatrix} = \begin{bmatrix} \mathbf{v}_i \\ -\frac{\mu \mathbf{r}_i}{|\mathbf{r}_i|^3} \end{bmatrix} \quad (1)$$

where $i=1, 2$ represent the target satellite and track satellite, $\mathbf{r}_i=[x_i, y_i, z_i]$, $\mathbf{v}_i=[v_{xi}, v_{yi}, v_{zi}]$ are the position vector and velocity vector, respectively, and $r_i = \|\mathbf{r}_i\|$; $\mathbf{u}_i=[u_{xi}, u_{yi}, u_{zi}]$ is the acceleration caused by the thrusters for formation-keeping; μ is lunar gravitational constant.

Following the navigation measurement of [1], the relative inertial-position measurement \mathbf{Z} is utilized and the measurement noise \mathbf{v} is assumed as uncorrelated zero-mean identity-covariance Gaussian random vectors. Then, the measurement model is written as:

$$\mathbf{Z} = (\mathbf{r}_1 - \mathbf{r}_2) + \mathbf{v} = \mathbf{H}\mathbf{X} + \mathbf{v} \quad (2)$$

where \mathbf{v} has known covariance matrices \mathbf{Q} ; $\mathbf{X}=[\mathbf{r}_1^T, \mathbf{v}_1^T, \mathbf{r}_2^T, \mathbf{v}_2^T]^T$ is the state vector; \mathbf{H} is the observation matrix, and its value is:

$$\mathbf{H} = \begin{bmatrix} 1 & 0 & 0 & 0 & 0 & 0 & -1 & 0 & 0 & 0 & 0 & 0 \\ 0 & 1 & 0 & 0 & 0 & 0 & 0 & -1 & 0 & 0 & 0 & 0 \\ 0 & 0 & 1 & 0 & 0 & 0 & 0 & 0 & -1 & 0 & 0 & 0 \end{bmatrix} \quad (3)$$

3 Numerical analysis method

3.1 Adaptive unscented Kalman filter

Based on dense-output Runge-Kutta numerical integration of the state dynamics differential equation (1), the dynamic propag-

ation from k to $k+1$ is developed. Then, the discrete-time non-linear dynamic modeling of satellite formation-flying system can be written as

$$\begin{cases} \mathbf{X}_k = f(\mathbf{X}_{k-1}, \mathbf{u}_k) + \mathbf{w}_{k-1} \\ \mathbf{Z}_k = \mathbf{H}_k \mathbf{X}_k + \mathbf{v}_k \end{cases} \quad (4)$$

where f is the vector-valued state prediction function; k is the discrete-time index; The process noise \mathbf{w}_k is considered to be uncorrelated, white, and Gaussian with zero mean and known covariance matrices \mathbf{R} . Besides, the process noise and the measurement are uncorrelated to each other.

It is also assumed that the initial state, $\hat{\mathbf{X}}_0$, is known with corresponding uncertainty given by the initial error covariance matrix \mathbf{P}_0 . Next, the unscented Kalman filter (UKF) is proposed to solving this type of problem is utilized.

The main UKF algorithm is as follows.

Step 1: Determine scaling and weights

$$\begin{cases} \alpha, \beta, \kappa \\ \lambda = \alpha^2(L + \kappa) - L \\ \eta_0^m = \lambda / (L + \lambda) \\ \eta_0^c = \lambda / (L + \lambda) + 1 - \alpha^2 + \beta \\ \eta_i^m = \eta_i^c = 1 / [2(L + \lambda)], i = 1, \dots, 2L \end{cases} \quad (5)$$

where α , β and κ are scaling parameters [14], λ is the additional scaling parameter, η^m (mean), η^c (covariance) are weight vectors, L is the length of the state vector.

Step 2: Define initial state error, initial state covariance, process and measurement noise covariance matrices

$$\begin{cases} \bar{\mathbf{X}}_0 = E(\mathbf{X}_0) \\ \mathbf{P}_0 = E((\mathbf{X}_0 - \bar{\mathbf{X}}_0)(\mathbf{X}_0 - \bar{\mathbf{X}}_0)^T) \\ \mathbf{Q}_k = E[\mathbf{w}_k \mathbf{w}_k^T] \\ \mathbf{R}_k = E[\mathbf{v}_k \mathbf{v}_k^T] \end{cases} \quad (6)$$

Step 3: Prediction transformation

$$\mathbf{x}_{k-1} = [\hat{\mathbf{X}}_{k-1} \quad \hat{\mathbf{X}}_{k-1} + \sqrt{(L+\lambda)\mathbf{P}_{k-1}} \quad \hat{\mathbf{X}}_{k-1} + \sqrt{(L+\lambda)\mathbf{P}_{k-1}}] \quad (7)$$

$$\mathbf{x}_{k|k-1}^{(i)} = f(\mathbf{x}_{k-1}^{(i)}, \mathbf{u}_{k-1}), \quad i = 0, 1, \dots, 2L \quad (8)$$

$$\hat{\mathbf{x}}_{k|k-1} = \sum_{i=0}^{2L} \eta_i^m \mathbf{x}_{k|k-1}^{(i)} \quad (9)$$

$$\mathbf{P}_{k|k-1} = \mathbf{Q}_{k-1} + \sum_{i=0}^{2L} \eta_i^c (\mathbf{x}_{k|k-1}^{(i)} - \hat{\mathbf{x}}_{k|k-1})(\mathbf{x}_{k|k-1}^{(i)} - \hat{\mathbf{x}}_{k|k-1})^T \quad (10)$$

$$\mathbf{x}_{k-1} = [\hat{\mathbf{X}}_{k-1} \quad \hat{\mathbf{X}}_{k-1} + \sqrt{(L+\lambda)\mathbf{P}_{k-1}} \quad \hat{\mathbf{X}}_{k-1} + \sqrt{(L+\lambda)\mathbf{P}_{k-1}}] \quad (11)$$

$$\mathbf{x}_{k-1} = [\hat{\mathbf{X}}_{k-1} \quad \hat{\mathbf{X}}_{k-1} + \sqrt{(L+\lambda)\mathbf{P}_{k-1}} \quad \hat{\mathbf{X}}_{k-1} + \sqrt{(L+\lambda)\mathbf{P}_{k-1}}] \quad (12)$$

Step 4: Observation transformation

$$\mathbf{P}_k^{xy} = \mathbf{R}_k + \sum_{i=0}^{2L} \eta_i^c (\Psi_{k|k-1}^{(i)} - \hat{\mathbf{Z}}_{k|k-1})(\Psi_{k|k-1}^{(i)} - \hat{\mathbf{Z}}_{k|k-1})^T \quad (13)$$

$$\mathbf{P}_k^{yy} = \sum_{i=0}^{2L} \eta_i^c (\mathbf{x}_{k|k-1}^{(i)} - \hat{\mathbf{X}}_{k|k-1})(\Psi_{k|k-1}^{(i)} - \hat{\mathbf{Z}}_{k|k-1})^T \quad (14)$$

Step 5: Measurement Update

$$\mathbf{K}_k = \mathbf{P}_k^{xy} (\mathbf{P}_k^{yy})^{-1} \quad (15)$$

$$\hat{\mathbf{X}}_k = \hat{\mathbf{X}}_{k|k-1} + \mathbf{K}_k (\mathbf{Z}_k - \hat{\mathbf{Z}}_{k|k-1}) \quad (16)$$

$$\mathbf{P}_k = \mathbf{P}_{k|k-1} - \mathbf{K}_k \mathbf{P}_k^{yy} \mathbf{K}_k^T \quad (17)$$

3.2 Numerical observability analysis

In this section, the linear observability analysis method of [15] is utilized to analyze the presented autonomous system. Compared with the Lie differentiation method, the above method is more simple and easy [16]. With the linear observability analysis method, the observability matrix of the discrete-time linear autonomous system is given by

$$\mathbf{M} = \begin{bmatrix} \mathbf{H}_k \\ \mathbf{H}_{k+1} \Phi(\mathbf{X}_k) \\ \mathbf{H}_{k+2} \Phi(\mathbf{X}_{k+1}) \Phi(\mathbf{X}_k) \\ \vdots \\ \mathbf{H}_{k+11} \Phi(\mathbf{X}_{k+10}) \Phi(\mathbf{X}_{k+9}) \dots \Phi(\mathbf{X}_k) \end{bmatrix} \quad (18)$$

where

$$\Phi(X_k) = \left. \frac{\partial f}{\partial X} \right|_{X=X_k}$$

Through diving the largest singular value of the observability matrix by the smallest singular value, the condition number is obtained. Then, the condition number of the observability matrix is developed to measure the degree of local observability. If the condition number is large, the observability matrix is close to singular and the system is weakly observable, even unobservable.

4. Simulation results and analysis

4.1 Initial condition

In this paper, the computation procedure is encoded in Matlab 7.0 and runs on a personal computer with a Intel(R) Core(TM) i5-4460 CPU (3.20 GHz) processor and two 4.00 GB RAM. In all simulations, the simulated initial state vector of target satellite is depicted in Table 1. Following the approach of Xing [17] and Elsaka [18], the satellite formation-flying is designed and table 2, 3 show the initial relative-state of track satellite, which are in different formation flying. The constants used in this study is $\mu=4.902801056 \times 10^{12} \text{ m}^3/\text{s}^2$. The planning period is 10000 s. Based on those simulation conditions, the relative position measurements are achieved.

Using the UKF algorithm method, the parameters, which including the orbits of twin satellites, are estimated. The filter has been initialized as follows: the initial state error is $X_0 = [1 \times 10^3, 1 \times 10^3, 1 \times 10^3, 1, 1, 1, 1 \times 10^3, 1 \times 10^3, 1 \times 10^3, 1, 1, 1]$; the initial state covariance matrices $P_0 = [1 \times 10^6, 1 \times 10^6, 1 \times 10^6, 1, 1, 1, 1 \times 10^6, 1 \times 10^6, 1 \times 10^6, 1, 1, 1]$; the process noise covariance matrices $Q = [1 \times 10^{-6}, 1 \times 10^{-6}, 1 \times 10^{-6}, 1 \times 10^{-10}, 1 \times 10^{-10}, 1 \times 10^{-10}, 1 \times 10^6, 1 \times 10^6, 1 \times 10^6, 1 \times 10^{-10}, 1 \times 10^{-10}, 1 \times 10^{-10}]$; the measurement noise covariance matrices $R = [1 \times 10^{-2}, 1 \times 10^{-2}, 1 \times 10^{-2}]$; $\alpha=1, \beta=2, \kappa=0$ and $\rho=11$.

Table 1. The initial orbit elements of the target satellite

a/(km)	e/(°)	i/(°)	RAAN/(°)	w/(°)	u/(°)
1.80×10^6	0	0	0	0	0

Table 2. The initial relative-position vector of the track satellite in different formation-flying

Type	x/(m)	y/(m)	z/(m)
serial	0	1×10^4	0
horizontal circle	0	1×10^4	0
spatial circle	0	1×10^4	0
ACR-cartwheel	0	0	1×10^4

Table 3. The initial relative-velocity vector of the track satellite in different formation-flying

Type	$V_x/(\text{m} \cdot \text{s}^{-1})$	$V_y/(\text{m} \cdot \text{s}^{-1})$	$V_z/(\text{m} \cdot \text{s}^{-1})$
serial	0	-5.09×10^{-2}	0
horizontal circle	4.58	-5.73×10^{-2}	9.17
spatial circle	4.58	-5.09×10^{-2}	7.94
ACR-cartwheel	-1.83×10^{-1}	0	0

4.2 The observability analysis

Using the method in Section 3.2, the numerical results of the rank and the condition number of observability matrix M will be given. Fig 1 describes the ranks of observability matrix, which are in serial formation, spatial circle formation flying, horizontal circle formation flying and car-wheel formation flying, both equal 12 along with epoch increasing. Therefore, the presented autonomous systems in the four formation flying are observability. From Fig 1, it is obviously got that the rank of the observability matrix is 12 and concluded that the observable of the system in different formation could be preserved. Based on the theoretical observability analysis of Markley [5], the unobservable cases obey the following condition: the two spacecraft have identical altitude time histories. But, due to

the effect of the system noise, the designed serial formation flying in this paper is not ideal and the periodic oscillation is occurring in selenocentric distance (Fig 2), and hence the presented autonomous system in serial formation flying is observable.

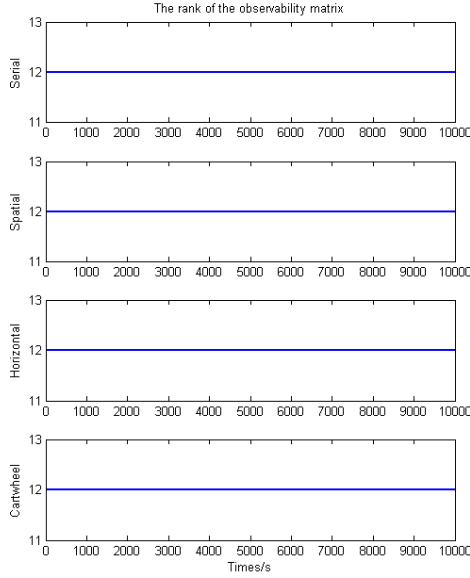


Fig. 1. The ranks of observability matrix in different formation flying

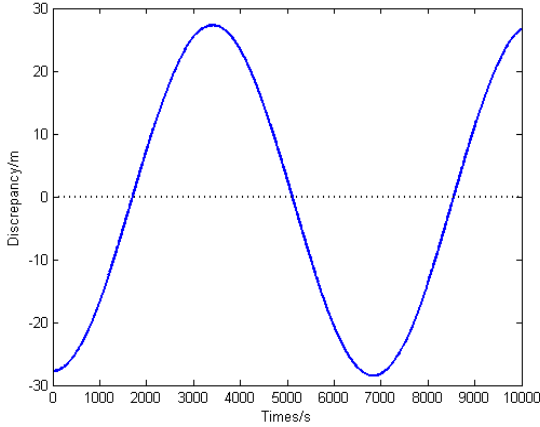


Fig. 2. the periodic oscillation of selenocentric distance discrepancy between two satellites

Table 4 lists the condition number of observability matrix in different formation flying. It shows the condition number in serial formation flying is the largest and the car-wheel formation flying has the least condition number. And the condition numbers in spatial circle formation and horizontal circle formation have the approximate equal value. Therefore, the above system in car-wheel formation flying has the best observability and it is the best formation-flying to get high navigation accuracy. Compared with the

other formation flying, the serial formation flying is the worst formation flying in the presented systems. Fig 3 shows the condition number of observability matrix in serial formation flying, spatial circle formation flying, horizontal circle formation flying and car-wheel formation flying. From Fig 3, the condition number curves of observability matrix are periodic oscillation.

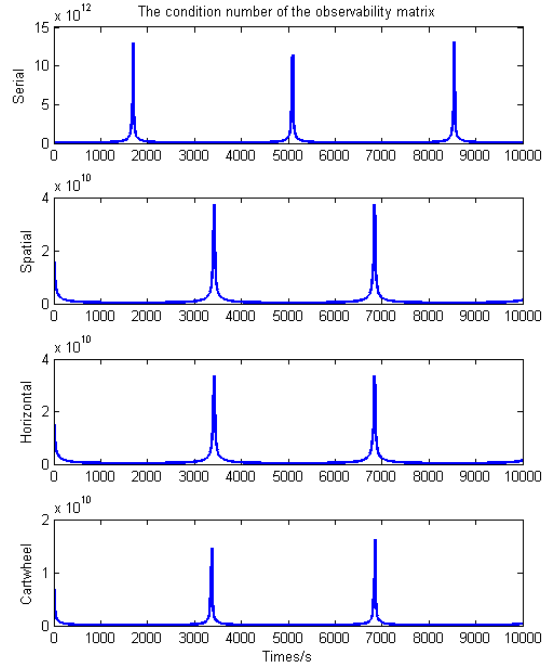


Fig. 3. Condition number of observability matrix in different formation flying

Table 3. The condition number of observability matrix in different formation flying

Type	Condition number
Serial formation flying	$5.79 \times 10^{10} \sim 1.31 \times 10^{13}$
Spatial circle formation flying	$3.29 \times 10^8 \sim 3.73 \times 10^{10}$
Horizontal circle formation Flying	$3.29 \times 10^8 \sim 3.35 \times 10^{10}$
Car-wheel formation flying	$8.19 \times 10^8 \sim 1.61 \times 10^{10}$

The time and selenocentric distance in the peak value of spatial circle formation flying is depicted in Table 5. Then, through Table 6, it is concluded that the violent oscillation of condition number is occurring when the two satellite have the identical selenocentric distance. Moreover, Table 6 lists the motion period and

the interval of the two peak value in the different formation flying, the oscillation period is almost the half of the motion period. Based on Table 5 and 6, the conclusion that the above system has low observability when the two satellites have the equal selenocentric distance could be achieved.

Table 5 The times and selenocentric distance in the peak value

Type		Peak 1	Peak 2
Time(s)		3420	6840
Selenocentric	Target	1.80×10^6	1.80×10^6
	Track	1.80×10^6	1.80×10^6

Table 6 The motion period and the interval of the two peak value in the three solutions

Type	the motion period (s)	the mean interval (s)
Serial formation flying	6852.78	3425.00
Spatial circle formation flying	6852.78	3420.00
Horizontal circle formation flying	6852.78	3420.00
Car-wheel formation flying	6852.78	3485.00

4.3 The results analysis

For autonomous system in each formation-flying, the initial conditions were described in Section 4.1. The performance was compared using the root mean-square error (RMSE) defined by

$$\text{RMSE} = \sqrt{\frac{1}{N} \sum_{k=1}^N (\hat{\mathbf{x}}_k - \mathbf{x}_k)^T (\hat{\mathbf{x}}_k - \mathbf{x}_k)} \quad (19)$$

where N is the iteration number; $\hat{\mathbf{x}}_k$ is the estimation position vector of target vector; \mathbf{x}_k is the real position vector of target vector.

When the measurement noise is considered to be uncorrelated, white, and Gaussian with zero mean and known covariance matrices, only UKF algorithm is utilized to estimate the navigation parameter. The RMSEs of 100 Monte-Carlo runs are depicted in Fig 4. In Fig 4, the

RMSE of car-wheel formation flying is by smaller than that of any formation flying, which indicates car-wheel formation is the best formation flying to get high navigation accuracy. Fig 5 shows the mean and standard variance of RMSEs. And Table 7 lists the specific value of the mean and standard variance. The value of mean and standard variance in serial formation flying is largest, which is obviously distinguishable from the values in other formation-flying. And the spatial circle formation flying is the second largest in RMSEs. The value in horizontal circle formation is slightly smaller than the value in the spatial circle formation flying. Finally, the car-wheel formation flying comes as fourth. We see that the simulation results agree rather well with the observability analytical conclusion in Section 4.2 and show the above prediction is right.

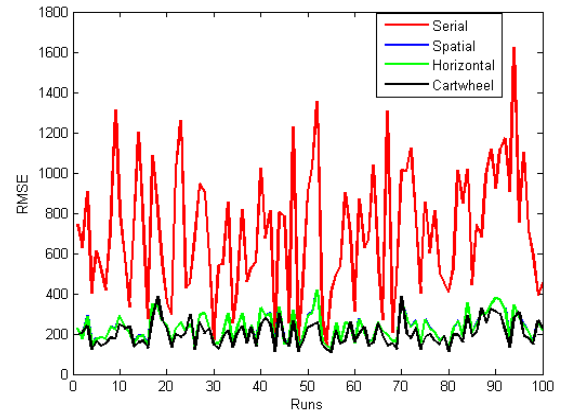


Fig. 4. RMSEs of each formation-flying across 100 random runs

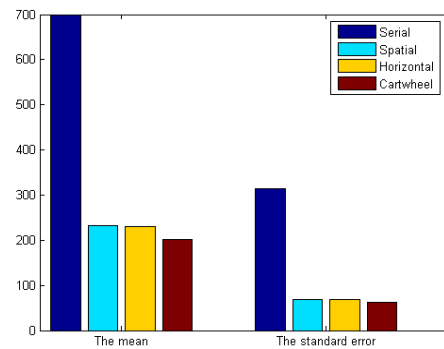


Fig. 5. Mean and standard variance of RMSEs across 100 random runs

Table 6. Mean and standard variance of RMSEs across 100 random runs

Type	mean (m)	Standard variance (m)
Serial formation flying	699.03	314.20
Spatial circle formation flying	231.83	69.36
Horizontal circle formation flying	230.54	69.53
Car-wheel formation flying	202.10	61.56

5. Conclusions

Combining the technologies of the satellite formation flying with the satellite to satellite tracking (SST), a novel intensification method selecting the available spacecraft formation flying to increase the navigational precision is proposed. Considering the effect of satellite formation flying, the autonomous navigation system with relative inertial-position vector measurement is proposed firstly. Then, observability of the system with the available measurements is investigated using the linear observability analysis, and the absolute state variable observability is obtained, excepting for quite a few special situations. Using UKF algorithm method, the accuracies of state estimation in different satellite formation flying, such as collinear formation, projection circular formation, space circular formation and Along-Cross-Radial(ACR)-Cartwheel formation, is investigated. It can be concluded from the analysis that the ACR-Cartwheel formation flying is more effective and efficient in dealing with autonomous navigation problem. Lastly, the results are confirmed through the 100 Monte-Carlo simulations.

Acknowledgements

This work was supported by the National Natural Science Foundation of China (Grant no 11302253). The authors thank Xing Jianjun and

Yu Jing for their helpful suggestion and revision to improve this paper.

References

- [1] Psiaki M L. Absolute orbit and gravity determination using relative position measurements between two satellite. *Journal of Guidance, Control, and Dynamics*, Vol. 34, No. 5, pp 1285-1297, 2011.
- [2] Wang Y, Xing J J, Zheng L M, et al. Autonomous determination of lunar gravity constant and coefficient of the lunar J_2 perturbation based on adaptive Kalman filter. *Journal of Astronautics*, Vol. 36, No. 7, pp 777-783, 2015.
- [3] Quadrelli M B, Wood L J, Riedel J E, et al. Guidance, navigation, and control technology assessment for future planetary science missions. *Journal of Guidance, Control, and Dynamics*, Vol. 38, No. 7, pp 1165-1186, 2015
- [4] Ning X L, Wang L H and Bai X B. Autonomous satellite navigation using starlight refraction angle measurements. *Advance in Space Research*, Vol. 51, No. 9, pp 1761-1772, 2013.
- [5] Mark F L. Autonomous navigation using landmark and intersatellite data. *AIAA/AAS Astrodynamics Conference*, Seattle, Washington, 1984.
- [6] Psiaki M L. Autonomous orbit determination for two spacecraft from relative position measurements. *Journal of Guidance, Control, and Dynamics*, Vol. 22, No. 2, pp 305-312, 1999.
- [7] Xiong K, Wei C L and Liu L D. The use of X-ray pulsars for aiding navigation of satellites in constellations. *Acta Astronautica*, Vol. 64, No. 4, pp 427-436, 2009.
- [8] Sun J, Zhang S J, Li B, et al. Autonomous navigation based on star light and ultraviolet earth sensors. *Optics and Precision Engineering*, Vol. 21, No. 4, pp 1192-1198, 2013.
- [9] Wang Y D, Zheng W and Sun S M. X-ray pulsar-based navigation system with the errors in the planetary ephemerides for earth-orbiting satellite. *Advances in Space Research*, Vol. 51, No. 12, pp 2394-2404, 2013.
- [10] Yang W B, Li S Y and Li N. A switch-mode information fusion filter based on ISRUKF for autonomous navigation of spacecraft. *Information Fusion*, Vol. 18, pp33-42, 2014.
- [11] Maryam K, Seid H P. Orbit determination via adaptive Gaussian swarm optimization. *Advances in Space Research*, Vol. 55, No. 4, pp 1028-1037, 2015.
- [12] Shen Y H, Xu L P, Zhang H, et al. Relative orbit determination for satellite formation flying based on quantum ranging. *Advances in Space Research*, Vol. 56, No. 4, pp 680-692, 2015.
- [13] Wang Y, Xing J J, Yu Y, et al. Autonomous lunar gravitational field determination via relative position measurement of the satellite formation. *Computer*

Engineering & Science, Vol. 38, No. 1, pp 125-130, 2016.

- [14] Julier S J, Uhlmann J K. New extension of the Kalman filter to nonlinear systems. *Proceedings of SPIE: The International Society for Optical Engineering*, Vol 3068, pp 182-193, 1997.
- [15] Chen Z. Local observability and its application to multiple measurement estimation. *IEEE Transactions on Industrial Electronics*, Vol 38, No 6, pp 491-496, 1991.
- [16] Chen T, Xu S J. Double line-of-sight measuring relative navigation for spacecraft autonomous rendezvous. *Acta Astronautica*, Vol 67, No 1, pp 122-134, 2010.
- [17] Xing J J. Study on formation design and stationkeeping of spacecraft formation flying. Changsha: National University of Defense Technology, 2007.
- [18] Elsaka B. Simulated multiple formation flights for future gravity field recovery. Bonn: University of Bonn, 2010..

Contact Author Email Address

Contact author: Yuzhu Bai
Email: baiyuzhu@hotmail.com

Copyright Statement

The authors confirm that they, and/or their company or organization, hold copyright on all of the original material included in this paper. The authors also confirm that they have obtained permission, from the copyright holder of any third party material included in this paper, to publish it as part of their paper. The authors confirm that they give permission, or have obtained permission from the copyright holder of this paper, for the publication and distribution of this paper as part of the ICAS proceedings or as individual off-prints from the proceedings.